European Journal of Cell Biology 101 (2022) 151274

Contents lists available at ScienceDirect

European Journal of Cell Biology

journal homepage: www.elsevier.com/locate/ejcb

Epithelial cell cluster size affects force distribution in response to EGF-induced collective contractility

Chiara Zambarda [a,1], Carlos Pérez González [b,c], Andreas Schoenit [a,2], Nisha Veits [a], Clara Schimmer [a], Raimund Jung [a], Dirk Ollech [a,1], Joel Christian [a], Pere Roca-Cusachs [b,c], Xavier Trepat [b,c,d,e], Elisabetta Ada Cavalcanti-Adam [a,*]

[a] Max Planck Institute for Medical Research, Jahnstr. 29, D-69120 Heidelberg, Germany
[b] Institute for Bioengineering of Catalonia (IBEC), The Barcelona Institute of Technology (BIST), Barcelona, Spain
[c] University of Barcelona, Barcelona, Spain
[d] Institució Catalana de Recerca i Estudis Avançats, Barcelona, Spain
[e] Centro de Investigación Biomédica en Red de Bioingeniería (CIBER-BBN), 08028 Barcelona, Spain

ARTICLE INFO

Keywords:
Collective contractility
Actomyosin
EGF
Traction forces
Adherens junctions
Micropatterning

ABSTRACT

Several factors present in the extracellular environment regulate epithelial cell adhesion and dynamics. Among them, growth factors such as EGF, upon binding to their receptors at the cell surface, get internalized and directly activate the acto-myosin machinery. In this study we present the effects of EGF on the contractility of epithelial cancer cell colonies in confined geometry of different sizes. We show that the extent to which EGF triggers contractility scales with the cluster size and thus the number of cells. Moreover, the collective contractility results in a radial distribution of traction forces, which are dependent on integrin β1 peripheral adhesions and transmitted to neighboring cells through adherens junctions. Taken together, EGF-induced contractility acts on the mechanical crosstalk and linkage between the cell-cell and cell-matrix compartments, regulating collective responses.

1. Introduction

Collective dynamics is central for epithelial tissue integrity maintenance and its perturbation leads to diseases, such as cancer cell growth and dissemination. In maintaining the cohesion of collectives, many cells individually correlate their own mechanical status with the one of their neighbors (Tambe et al., 2011). This complex force balance is regulated by intracellular biochemical signaling pathways, orchestrated by molecular complexes involved in cell-cell and cell-matrix adhesions (Mui et al., 2016). How these local chemo-mechanical signals are integrated and adjusted at the multicellular level remains still largely unknown.

Cell-cell adhesion is facilitated by adherens junctions (AJs), in which the cadherin-catenin complex is crucial for sensing and transducing forces, as well as for adapting to forces experienced by cells during epithelial collective dynamics (Han et al., 2016; Pannekoek et al., 2019). Mechanotransduction at intact AJs allows cells to respond to chemo-mechanical signals of the environment through activation of myosin II contractility (Seddiki et al., 2018). Recent findings suggest that in multicellular clusters, stresses at nearby AJs are tightly coupled and directly contribute to the transmission of forces exerted at matrix contacts. Cell-cell and cell-matrix adhesion sites are mechanically coupled through a pre-stressed actin network, which allows to balance adhesive forces to adjust to cell shape changes (Maruthamuthu et al., 2011) and, within a cluster for each cell forces are balanced at AJs and focal adhesions (FAs). When adhesive forces at AJs are weakened through a perturbation of cell-cell contacts, cell-matrix forces are reorganized, shifting from ring-like traction at the periphery to high and evenly distributed forces across the cell cluster (Mertz et al., 2013).

Soluble growth factors such as epidermal growth factor (EGF), alter epithelial cells morphology and mechanics (Chinkers et al., 1979; Yang et al., 2012) and induce actin polymerization and migration of different

* Corresponding author.
E-mail address: eacavalcanti@mr.mpg.de (E.A. Cavalcanti-Adam).
[1] **Present address:** Science for Life Laboratory and KTH Royal Technical University, Applied Physics Department, Tomtebodavägen 23A, S-17165 Stockholm, Sweden.
[2] **Present address:** Institut Jacques Monod, CNRS and Université de Paris, 75013 Paris, France.

https://doi.org/10.1016/j.ejcb.2022.151274
Received 29 December 2021; Received in revised form 8 August 2022; Accepted 8 September 2022
Available online 17 September 2022

cancer cell types (Felkl et al., 2012; Makowiecka et al., 2016). Additionally, EGF activates ROCK, leading to phosphorylation of myosin II regulatory light chain and inactivation of myosin II phosphatases (Rubsam et al., 2017). As a result, there is an increase in myosin II contractility, which initially triggers stress fiber assembly and an increase in traction forces. Of note, maturation of adhesions to the matrix is guided by actin stress fiber assembly even in absence of tension due to myosin II activation (Choi et al., 2008; Oakes et al., 2012; Stricker et al., 2011). At FA, upon EGF stimulation, there is a decrease in adhesion strength to the matrix due to paxillin dephosphorylation and subsequent retraction of protrusions (Schneider et al., 2009). In cell clusters, the level of complexity for integrating signaling into mechanical responses is increased due to the presence of AJs, which act themselves as mechanical units. By using a finite element model to resolve 3D traction forces in epithelial cell clusters, it was shown that the magnitude of tractions within the cluster increases in response to EGF and that the cluster behaves like a spring-like single unit, where maintenance of tension at cell-cell junctions coordinates the collective response (Notbohm et al., 2012). In this model, two different tractions were presented: In-plane tractions pulling on the substrate directed to the center of the cluster, and larger out-of-plane tractions, occurring due to structural reorganization of the cluster. While these studies point out the importance of the mechanotransducive properties of AJs in maintaining collective integrity, it remains to be identified how the force balance at cell-cell and cell-matrix adhesions is maintained during EGF-induced collective contractility.

Here, we use surface patterning and biophysical approaches to analyze static confined monolayers of epithelial carcinoma cells at a constant surface density. We show that EGF-mediated contractility results in a transition from flat to dome-like cell collectives, which requires intact AJs. Increasing monolayer size leads to an increase in traction forces and modulates the internal stress distribution. Triggering collective contractility, EGF induces the actomyosin-dependent increase of collective forces which leads to a molecular clutch-mediated responses at FAs and is followed by retraction at matrix adhesions and overall cluster contractility.

2. Material and methods

2.1. Surface micropatterning

Surfaces were micropatterned using a protocol adapted from Azioune et al. (2010). Glass coverslips (20×20 mm^2 1.5, Carl Roth) were cleaned in 96 % ethanol for 15 min while sonicating, rinsed twice with deionized water and dried with an air gun. The coverslips were placed inside an ultraviolet light-ozone (UVO) cleaner (UVO Cleaner Unit 342, Jelight Company Inc., USA) for 10 min and afterwards their surface was coated with PLL-PEG (0.1 mg/ml in 10 mM HEPES, pH 7.5) (SuSoS Surface Technology, Switzerland). For micropatterning, a quartz chromium photomask (Toppan Photomasks, Inc.) was designed with 8 identical squared fields, sized 15 × 15 mm^2; containing an array of circles of ranging from 20 to 500 μm in diameter, spaced 150 μm from each other. The photomask was washed with acetone and isopropanol, dried and activated in the UVO cleaner for 5 min. Directly after activation, the passivated glass coverslips were sandwiched with the photomask using 4 μl of deionized water. The samples were placed in the UVO cleaner for 5 min and then washed with deionized water for 10 min. If not used immediately for cell experiments, the micropatterned coverslips were kept overnight at 4 °C.

2.2. Polyacrylamide gel fabrication, coating and micropatterning

Polyacrylamide (PAA) gels were fabricated as described previously (Casares et al., 2015; Latorre et al., 2018; Perez-Gonzalez et al., 2019). Briefly, polyacrylamide gels of 6 kPa containing fluorescent beads were generated by mixing 76.71 % (w/v) HEPES (#H4034, Sigma) 10 mM pH 7.5, 18.74 % (v/v) acrylamide 40% (#161-0140, BIO-RAD), 3 % (v/v) bis-acrylamide (#161-0142, BIO-RAD), 1 % (v/v) Fluo-Spheres carboxylate-modified 0.2 μm red (Ex. 580, Em. 605) (#F8810, Invitrogen), 0.5 % (v/v) ammonium persulphate (APS) solution (10 %(v/v) APS (#A3678, SIGMA) in H2O) and 0.05 % (v/v) Tetramethylethylenediamine (TEMED) (#T9281, Sigma). The gel surface was activated with a solution of 2 mg/ml of Sulpho-SANPAH exposed to UV light of 365 nm for 5 min (#XX-15 L, Workflow Solutions for Life Science) to covalently crosslink extracellular matrix proteins. After washing with PBS, PDMS stencils containing circular openings of the desired sizes were placed on top to micropattern the adhesive regions. PDMS stencils were fabricated as described previously (Perez-Gonzalez et al., 2019). A solution of 100 μg/ml collagen type I (rat tail #08-115, Millipore) was added on top of the gel and incubated overnight at 4 °C. Before cell seeding, the samples were washed with PBS and the stencil was removed.

2.3. A431 cell culture

Human epidermoid carcinoma cell line A431 was purchased from ATCC (#CRL-1555, LOT: 60304745). CRISPR-Cas9 A431 α-catenin knockout cells and rescue transfected with pLV-α-catenin-mCherry were kindly provided by Takuya Kato (F. Crick Institute, London) (Labernadie et al., 2017). All cell lines were cultured at 37 °C in 5% CO_2 in complete growth medium, containing high glucose DMEM, (#41966 Thermo Fisher), 10 % FBS and 1 % Pen/Strep (Thermo Fischer). Confluent cells were passaged at 1:3 dilution using 0.25 mM trypsin/EDTA (Thermo Fischer) for detachment. For experiments on micropatterned glass coverslips, cells were seeded at a density of 8.3×10^4 cell/cm^2. For the TFM experiments on PAA hydrogels, 10^6 cells were resuspended in 200 μl of complete medium and seeded on the hydrogel surfaces for 20 min. Then, unattached cells were removed by vigorous washing with sterile PBS and the remaining cells were grown in complete medium.

2.4. EGF and blebbistatin treatment

A431 cells were seeded on the samples in complete growth medium for 48 h. Then, cells were washed twice with PBS and serum starved using DMEM without FBS, supplemented with 1 % Pen/Strep for 5 h. Recombinant human epidermal growth factor (EGF; # 236-EG, R&D) was added to the starvation medium at a concentration of 100 ng/ml in PBS. As negative control, an equivalent amount of PBS was added to the media. For myosin II inhibition experiments, the cells were treated for 1 h with blebbistatin (#B0560-5MG, Sigma Aldrich) dissolved in dimethyl sulfoxide (DMSO) at a concentration of 50 μM. As negative control, an equivalent amount of DMSO was added to the media.

2.5. Western blot

A431 cells, A431 α-catenin knockout cells and rescue transfected α-catenin knockout cells were grown as previously described. Cells were then washed with cold PSB, lysed with RIPA lysis buffer supplemented with 1 % (v/v) Halt Protease and Phosphatase Inhibitor Single-Use Cocktail and 1 % (v/v) 0.5 M EDTA and incubated overnight at − 80 °C. The following day cell lysates were collected and centrifuged (14,000 rpm for 30 min at 4 °C). Protein containing supernatants were processed according to NuPAGE™ Bis-Tris Mini Gels protocol (Thermo Fisher). After protein transfer, nitrocellulose membranes were blocked with 3 % BSA in TBS-T buffer and incubated with primary antibody solution (1 % BSA in TBS-T buffer) overnight at 4 °C. The following primary antibodies were used: 0.1 μg/ml α-catenin (Ab51032, Abcam), 0.5 μg/ml β-actin (A1978, Merck), 0.25 μg/ml β-catenin (610153, BD Bioscience), 0.2 μg/ml E-cadherin (Sc-8426 Santa Cruz), 0.2 μg/ml EGFR (Sc-03, Santa Cruz). The following day, three washing steps were performed followed by incubation with secondary antibody solution (1 % BSA in TBS-T buffer) at RT for 2 h. 0.4 μg/ml HRP conjugated anti

mouse (Sc-2005, Santa Cruz) or anti rabbit (Sc-2004, Santa Cruz) were used as secondary antibodies. The membranes were then washed three times with TBS-T and incubated with ECL Prime detection reagent (Amersham, GE Healthcare) to record the chemiluminescent signal using an imaging analyzer (Imager 600, Amersham).

2.6. Time-lapse microscopy

Time lapse phase contrast imaging was performed on a DeltaVision system (GE Healthcare) installed on an Olympus IX inverted fluorescence widefield microscope, with a cooled CCD camera (Coolsnap HQ, Roper Scientific, USA). A 10 × objective (NA 0.3, Zeiss) was used and images were obtained every 15 min over a period of 24 h.

The paxillin-YFP plasmid was kindly provided by Benjamin Geiger (the Weizmann Institute of Science, Rehovot) and cell transfection was performed using Amaxa cell line nucleofector (Kit T, Lonza). After transfection, 1×10^6 cells were seeded in complete medium on micropatterned glass surfaces for 24 h and then treated with EGFR as previously described. Time lapse was performed in DMi8 inverted fluorescence widefield microscope (Leica) using a 63 × oil objective (NA 1.4, Leica). Images were acquired every minute starting 5 min prior to EGF stimulation over a period of 1 h.

To label the actin cytoskeleton, A431 cells on micropattern were rinsed with warm PBS. SiR actin and verapamil (catalog no. SC001, Spirochrome, diluted 1:1000) were added to the medium and cells were incubated for 1 h at 37 °C and 5 % CO_2. Immediately following addition of EGF, images were acquired every 5 min at room temperature using a laser scanning confocal microscope (Zeiss LSM 900, Oberkochen, Germany) equipped with a 20 × air (Objective Plan-Apochromat 20 ×/0.8 M27, Carl Zeiss AG).

2.7. Traction force microscopy and monolayer stress microscopy

For traction force microscopy (TFM), an inverted fluorescence widefield DMi8 microscope (Leica) equipped with a dark incubation chamber controlling a temperature and CO_2 was used. Images were acquired with 10 × objective and using the software LAS X (Leica). Alternatively, samples were imaged with an automated inverted fluorescence widefield microscope (Nikon Eclipse Ti2) with 20 × objective. The microscope was operated with the software MetaMorph (Universal Imaging).

Traction forces were computed as previously described (Perez-Gonzalez et al., 2019; Trepat et al., 2009). Briefly, bead displacements were measured by comparing each bead image of the time-lapse to a reference image of the relaxed gel after removing cells by adding of trypsin. Substrate displacement maps were calculated using custom-made particle image velocimetry (PIV) implemented in Matlab. Traction forces were calculated from substrate displacements using Fourier Transform Traction Force Microscopy with a finite gel thickness (Trepat et al., 2009).

Monolayer internal stresses were computed from traction maps using monolayer stress microscopy as previously described (Tambe et al., 2011). The average normal stress was computed as the mean of the *xx* and *yy* components, as the increase in tension triggers the transition while the cluster is still a monolayer. 2D force balance provides stresses in the units of surface tension (N/m). To provide stresses in Pa, a constant monolayer thickness of 10 μm was assumed.

2.8. Immunofluorescence microscopy

Cells were fixed with 4 % (w/v) paraformaldehyde for 15 min and then washed twice with PBS. For immunofluorescence, plasma membrane was permeabilized with 0.1 % (v/v) Triton X-100 for 5 min. Samples were incubated with blocking solution (1 % bovine serum albumin (BSA) in PBS) for 30 min at RT. Staining with primary antibody was performed overnight at 4 °C, followed by incubation with secondary antibody for 2 h at RT. After each antibody incubation step the samples were washed three times for 10 min each. The coverslips were mounted in Mowiol containing DABCO. Primary antibodies (α-catenin, 1:100, #Ab51032, Abcam; E-cadherin 1:200, # Sc-7870, Santa Cruz; β-catenin 1:500 #610153, BD Bioscience; paxillin Y118, #2541S, Cell Signaling; vinculin 1:100, #V9131, Sigma Aldrich; zyxin 1:100, #307011, Synaptic systems; integrin β1 clone 12G10 1:100 #30394 Abcam; pMLC2 1:50, #3671 S, Cell Signaling) were diluted in blocking solution and incubated on the samples overnight at 4 °C. Samples were incubated with secondary antibodies (AlexaFluor647 anti-mouse, 1:500 #A-21236, Thermo Fisher; AlexFluor488 anti-rabbit, 1:500, #A-11034, Thermo Fisher) in blocking solution for 1 h at RT. F-actin staining was done by using Phalloidin-TRITC (1:1000, #P1951, Sigma Aldrich). For fluorescent staining of plasma membrane, cells were fixed as described above and then incubated in blocking solution for 30 min at RT. The samples were incubated with 5 μg/ml wheat germ agglutinin conjugated with AlexaFluor488 (WGA, #W11261, Thermo Fisher) and 1 μg/ml DAPI (#D9542, Sigma Aldrich) for 30 min at RT. Cells were washed with blocking solution three times for 10 min each and mounted in Mowiol (Sigma-Aldrich) containing 1.4-diazabicyclo-[2.2.2]-octane (DABCO, Merck).

Cell proliferation was evaluated with the Click-iT EdU Flow Cytometry Cell Proliferation Assay (Thermo Fisher) following the manufacturer's protocol. Briefly, cells grown on glass coverslips were fixed in 4 % PFA for 15 min and washed with 3 % BSA in PBS for 10 min. Cells were then permeabilized with 0.5 % Triton-X 100 in PBS for 20 min. Cells were washed twice with washing solution and incubated in a buffer containing $CuSO_4$, AlexaFluor488 azide and reaction buffers for the click reaction for 30 min. Cells were washed and stained with 1 μg/ml DAPI for 15 min.

Epifluorescence images of fixed samples were acquired with an upright fluorescence widefield microscope (Leica DM6000B) with 40x and 63x objective and using the software LASX. Confocal images of fixed fluorescent samples were recorded with a LSM 880 and LSM 800 confocal microscopes (Zeiss) using the 40x and 63x objectives respectively. Fixed cells stained for actin, integrin β1 and pMLC were imaged with a laser scanning confocal microscope (Zeiss LSM 900, Oberkochen, Germany) equipped with a 63 × oil objective (Plan-Apochromat 63 ×/1.4 Oil DIC M27) using an Airyscan 2 module. Airyscan images were automatically post-processed using the Zeiss ZEN 2 software.

2.9. Image and statistical analysis

Nuclei counting of cell clusters was done using the plugin "*Nucleus Counter*" (ImageJ) for images processed by application in the following order of *Otsu algorithm/No Smooth filter/Subtract background/Watershed*. Since the algorithm underestimated the number of nuclei, automated count was manually corrected using *Show all* function in the ROI manager of *Cookbook* (ImageJ). For each cluster size the average number of nuclei was calculated. For statistical test, One-way ANOVA (GraphPad Prism 9) was performed. For the quantification of proliferating cells, EdU positive cells were manually counted in 3D z-stacks using the plugin *Cell count* (ImageJ). Statistical analysis was performed using unpaired t-test (GraphPad Prism 9). A431 cells cluster areas were quantified over time using the macro *MRI-wound healing tool* (ImageJ).

To quantify the area of FAs, fluorescence images of cell clusters stained for integrin β1 were automatically segmented using the random forest classifier Weka Segmentation (Arganda-Carreras et al., 2017). To train the classifier, approximately 100 FAs were annotated manually. The images were cropped in a way to only investigate integrin β1 clusters at the edge of the epithelial cell clusters (outer 5 μm) and a 2 × 2 median filter was applied. Binary images were generated and processed in ImageJ using *Analyse Particles* to obtain the area of each FA. Thereby, a size ($> 0.3\ \mu m^2$) and a circularity filter (< 0.7) were used to remove background and e.g. FAs merged due to the segmentation. To approximate the length and the ratio between the minor and the major axis,

ellipses were fitted on each detected cluster and their major and minor axes were measured. The results were verified by manual measurement of the FA length and width. Integrin cluster radial orientation analysis was performed by rotating the fields of view such that the cell cluster border is parallel to the x-axis. Next, images were cropped and a 5×5 median filter was applied. Binarized images were generated as described above and processed using the OrientationJ plugin in ImageJ (De Vos and Timmermans, 2016) to determine the distribution of integrin cluster orientation (Fig. S7). Time lapse movies of Paxillin-YFP were analyzed using the function *multi-kymograph* of ImageJ. Kymographs with a width of 8 pixel were plotted at the cell edge. Mean intensity values of the 8 pixel width were calculated for every timepoint using the *plot profile* function each kymograph and averaged. Multiple kymographs were merged to generate an average kymograph.

Using GraphPad Prism 9, a one-way ANOVA significance test with Welch's correction was performed on the means of the different experiments using Dunnett's multiple comparison test. Thereby, the threshold for significance was defined as $\alpha = 0.05$. p-values between 0.1 and 0.01 correspond to (*), p-values between 0.01 and 0.001 correspond to (**), p-values between 0.001 and 0.0001 correspond to (***) and p-values < 0.0001 correspond to (****). No statistical significance is denoted as (n. s.). The individual datapoints were plotted together with the results of the statistical analysis using GraphPad Prism 9.

3. Results

3.1. EGF-induced collective contraction dynamics depend on the size of epithelial cell clusters

To quantitatively examine the interplay between EGF-induced contraction and cell-cell junctions in regulating epithelial collective dynamics, we generated circular patterns with a diameter of 100–200–300 μm to grow defined clusters of human epidermoid carcinoma cells (A431 cell line) (Fig. 1). To generate cell clusters with defined size, surfaces were first coated with a layer of poly-L-lysine-polyethylene glycol (PLL-g-PEG) and then patterned by UV-photolithography, to create adhesive islands of different diameters. The PLL-g-PEG layer, visualized by conjugation to FITC fluorophore (Fig. 1A, upper row), prevents adhesion outside the adhesive area, thereby confining cells seeded on the substrate to defined regions

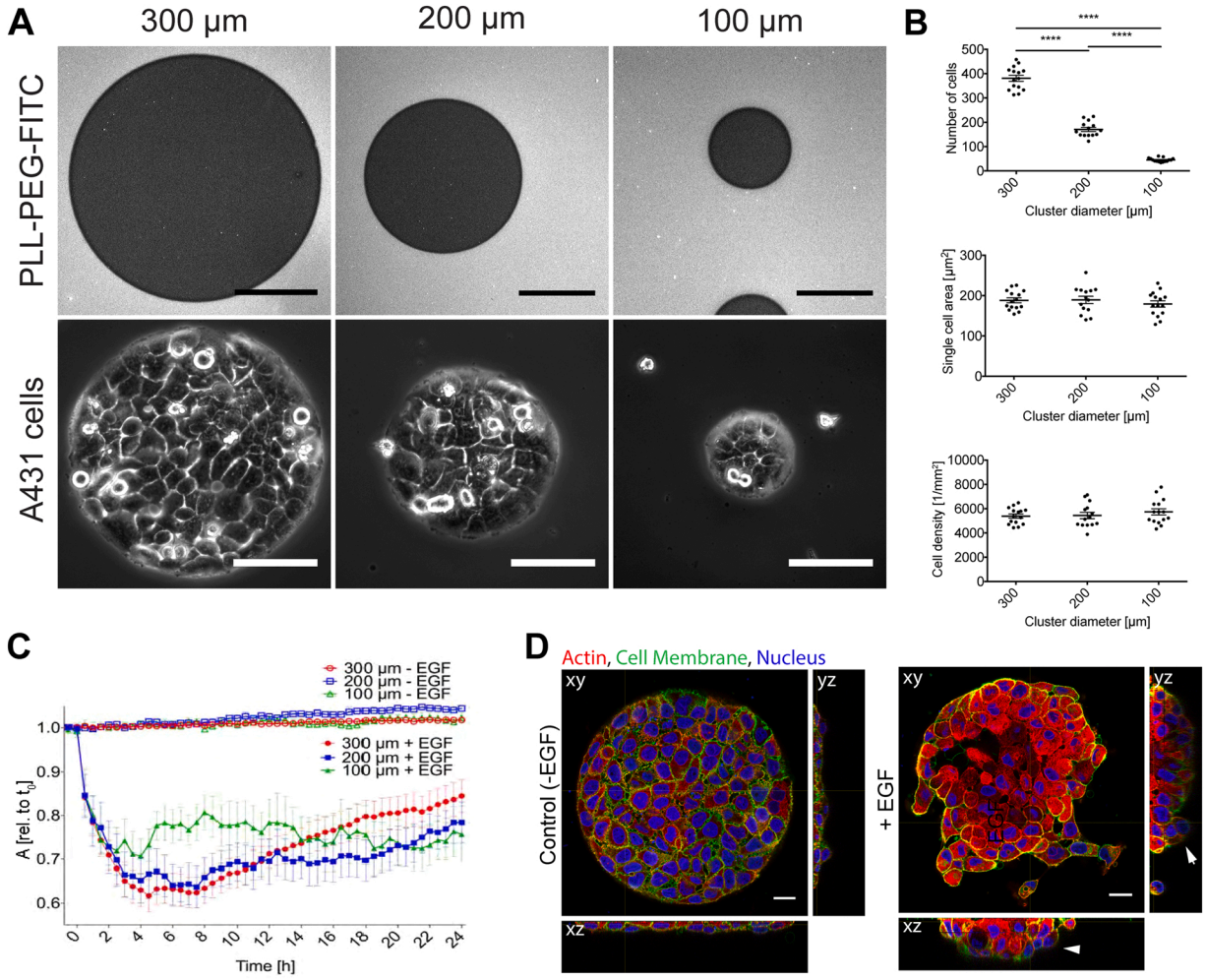

Fig. 1. EGF induces collective contractility of epithelial cell clusters. A, Glass surface micropatterning of A431 cell collectives arranged in circular clusters of 300–200–100 μm diameter. Upper row, passivated areas coated with PLL-PEG conjugated with FITC imaged by fluorescence microscopy. Lower row, clusters of cells adhering to the non-passivated regions imaged by phase contrast microscopy. Scale bar 100 mm. **B**, Quantification of cell number, single cell area and cell density for cell clusters of different size. Data from 3 independent experiments, N = 15, 14 and 15 for 300, 200 and 100 μm. Plots display median values (black line) ± SEM; **** $p < 0.0001$, Mann Whitney test. **C**, Changes in epithelial cell cluster area (normalized to initial cluster size) over time following addition of EGF (100 ng/ml) to the culture media or in absence of the growth factor (control). (N = 14, 11 and 9 for 300, 200 and 100 μm –EGF; N = 12, 10 and 9 for 300, 200 and 100 μm + EGF). Plots display the mean values ± SD for each time point. **D**, Confocal images of representative 200 μm-sized cell clusters in absence (control, -EGF) or in presence of EGF stained after 24 h for actin (red), cell membrane (green) and nucleus (blue) and orthogonal projections. The white arrow heads point cells that are piling up. Scale bar 20 μm.

(Fig. 1A, lower row). The number of adherent cells significantly varies with the size of the patterned region, being respectively 45 ± 2 for 100 μm, 170 ± 8 for 200 μm and 380 ± 12 for 300 μm (Fig. 1B, top). In contrast, single cell area (Fig. 1B, middle) and cell density (Fig. 1B, bottom) remain constant, where cells form a confluent monolayer within the patterned area. Cells were stimulated with 100 ng/ml EGF after having reached confluence. It should be noted that with this concentration of EGF, the number of proliferating cells was approximately 10% higher than the one observed for the untreated group (Fig. S1). Cells confined in the patterns and treated with 100 ng/ml EGF were immediately monitored by time lapse video-microscopy over a period of 24 h (Fig. 1C and Movie 1). Cluster area rapidly decreases only for EGF-treated cells in all cluster sizes within the first hour after addition of the growth factor to the media. For the first two hours of observation, cluster retraction is independent on the initial size of the adhesive islands. Afterwards, the size of the cell cluster on the 100 μm pattern remains unvaried over a period of 24 h, presenting a reduction of approximately 25 % of its original size. For the 200 and 300 μm clusters, the decrease in size for an additional reduction of approximately 35 % continues for 4 h, suggesting an additional mechanism responsible for the generation of forces underlying cluster dynamics. The rearrangement in cell cluster organization leads to piling up of cells and as a consequence, parts of the micropatterned circles are available for cells to adhere again to the substrate leading to recovery of the circular shape. Over a period of 24 h, a steeper recovery phase is observed for the 300 μm, whereas the 200 mm presented similar dynamics as for the 100 μm after 12 h observation, but with a faster recovery over time. These differences might be due to long-range multicellular dynamics present only in larger clusters and higher local cell density following cluster reorganization. Taken together, these results indicate that the response to EGF involves two phases, a first one independent on the monolayer size and a second one dependent on it. The retraction of EGF-treated clusters translates into a

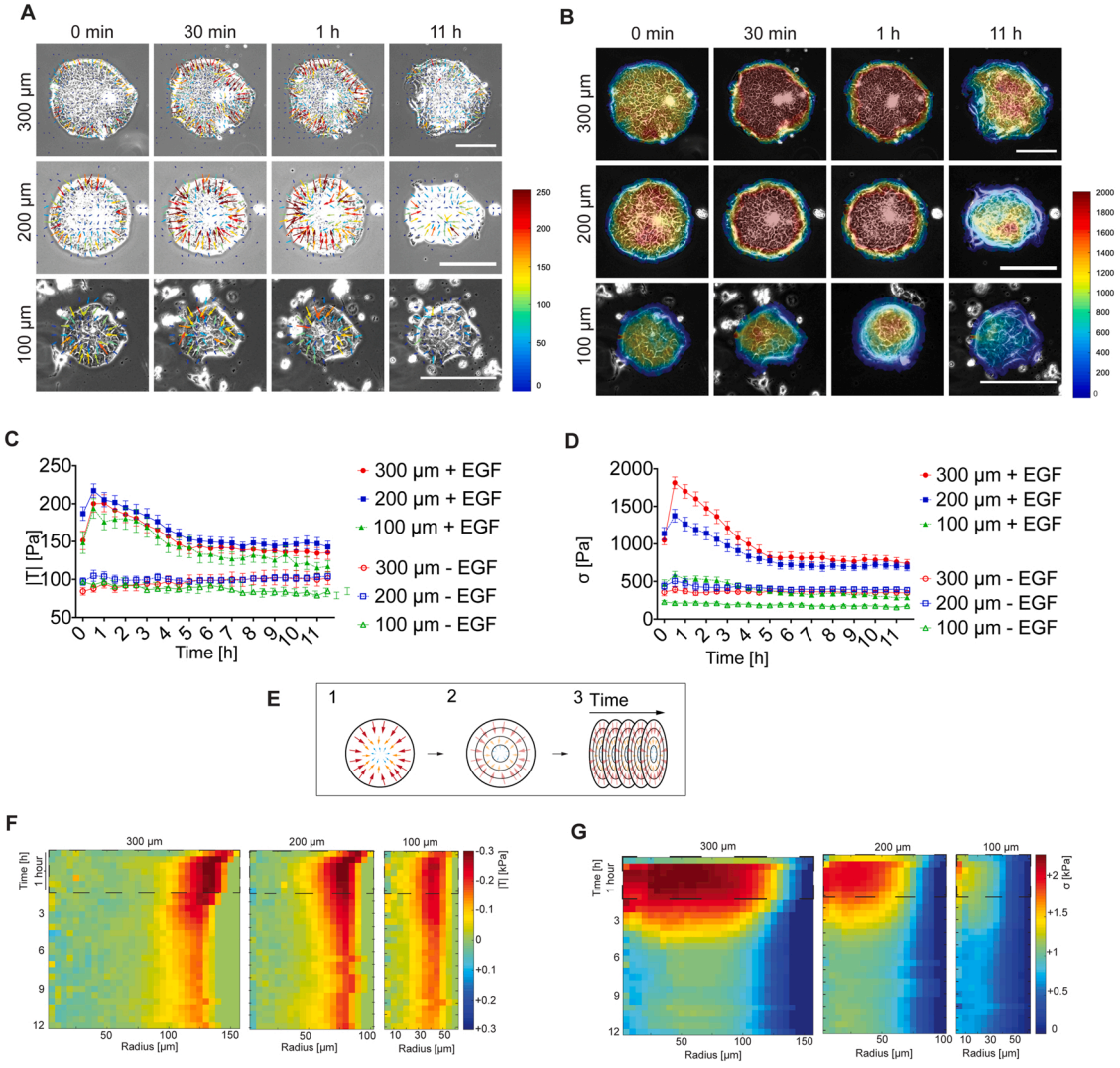

Fig. 2. Traction forces and internal stress rapidly increase in response to EGF. A, Traction forces maps overlay on cell clusters of 100–200–300 μm diameter. Low tractions are indicated with short arrows and cold colors, high tractions with long arrows and hot colors. Scale bar 100 μm. **B,** Maps of internal stress magnitude and distribution as function of cluster size. Color map shows in blue low internal stress and in dark red high internal stress. Scale bar 100 μm. **C,** Average traction values over time for clusters in absence or in presence of EGF. **D,** Average stress values over time for cell clusters in absence or in presence of EGF. For C and D, data from 4 independent experiments, N = 6, 18 and 8 for 300, 200 and 100 μm - EGF; N = 8, 21 and 14 for 300, 200 and 100 μm + EGF). Plots display mean ± SEM. **E,** Cartoon depicting the analysis workflow applied to resolve the radial distribution of traction forces (1), tractions recorded for each cluster were divided in radial zones with a step of 5 μm (2), average for each zone was calculated for each time point (3). **F**, Radial distribution of cell traction forces in clusters. Example kymographs for 300, 200 and 100 μm clusters. **G**, Radial distribution of internal stress. Example kymographs for clusters of different size. For F and G, the initial time interval is 10 min for the first hour (dashed line), followed by a 30-min time interval for the subsequent hours. Tractions are displayed as heat map where cold pixels indicate outward tractions and hot pixel denote inward tractions.

reorganization of the collective into a dome-like structure within the first 24 h (Fig. 1D). At the outer edge of the cluster, flat and extended cells emerge and reinvade the available space; at the same time, an extensive piling up of cells is observed starting from the periphery and increasing towards the cluster center. The changes in cluster shape appear to be a result of rounding up of the cell body, since after EGF treatment the clusters are no longer flat, as evidenced by indirect immunofluorescence staining (Fig. 1D).

Supplementary material related to this article can be found online at doi:10.1016/j.ejcb.2022.151274.

3.2. Cell collective reorganization in response to EGF-induced retraction is associated with a higher redistribution of traction forces and monolayer stress in larger clusters

To further elucidate the functional contribution of cell-cell and cell-matrix adhesions to epithelial cell cluster reorganization and retraction, we next determined the impact of monolayer size on traction forces exerted on the substrate following EGF stimulation (Fig. 2 and Movie 2). Cells were seeded on 6 kPa PAA hydrogels containing 200 nm-sized red fluorescent beads and micropatterned with collagen-coated adhesive islands to perform traction force microscopy and monolayer stress microscopy during EGF-induced cluster retraction (Fig. 2A and B). Collective dynamics in clusters of different sizes on PAA hydrogels were imaged by phase contrast video-microscopy and the cell area was quantified as described before (Fig. S2).

Supplementary material related to this article can be found online at doi:10.1016/j.ejcb.2022.151274.

Tractions were recorded for a period of 11 h following the addition of EGF to the culture media. Traction maps for all the cluster sizes revealed an increase in the magnitude of traction forces mainly at the cluster periphery (Fig. 2A), as indicated by the long and hot colored arrows. No significant difference in average traction magnitude is observed for the three different cluster sizes; while the peak of tractions at the edge is higher for larger patters, at the center of the pattern forces are low (Fig. 2 A and C). The increase in traction occurs within the first hour after EGF stimulation, followed by a gradual decrease in cell-generated tractions over time. Without EGF addition, cell clusters do not show any changes in traction over time.

We calculated the internal stress generated during collective retraction using monolayer stress microscopy (Tambe et al., 2013, 2011). The generated monolayer stress maps for epithelial cell clusters of different sizes were color-coded to indicate high (hot color) and low (cold color) stresses (Fig. 2B). The average monolayer stresses show a rapid and strong increase within the first hour of stimulation with EGF (Fig. 2D). The analysis of the temporal changes of monolayer stresses indicates that the initial increase observed after EGF addition scales according to the cluster size, with the 300 μm showing the highest values. Interestingly, a relaxation of internal stresses is observed 4 h after addition of EGF to all cell cluster sizes (Fig. 2D), after reaching increased local cell density due to rearrangement of the clusters.

To resolve the spatial distribution of traction forces generated by cells in clusters of different size, we performed traction force analysis divided in radial zones with steps of 5 μm in width. Tractions were then averaged and calculated for each time point (Fig. 2E). The radial distribution of cell traction forces over time indicates that, for all sizes, EGF induced an increase in tractions at the periphery (Fig. 2F). For the 200 and 300 μm clusters, the initial peripheral tractions are higher than for the 100 μm, but they decrease to a level comparable to the 100 μm after the first hour. The radial distribution of monolayer stresses also confirms that the increase triggered by EGF addition scales according to the cluster size (Fig. 2G). Taken together, these results demonstrate that the initial regulation of cell-matrix and cell-cell adhesion forces upon EGF-induced contraction of epithelial cell clusters depends on the cluster size.

3.3. Intact adherens junctions are required for force increase and cluster retraction due to EGF-induced contractility

To determine the impact of cell-cell junctions on the transmission of contractile forces in clusters of different sizes, we investigated the response to EGF in α-catenin knockout cells, which cannot form AJs (Fig. 3). At AJs, α-catenin acts as a connecting protein between the E-cadherin/β-catenin complex and the actin cytoskeleton (Fig. S3). The absence of α-catenin results in cytoplasmic retention and nuclear localization of β-catenin and a rearrangement of actin fibers and vinculin clusters at the cell periphery (Fig. S3A). A rescue transfection with full length α-catenin restores the localization of β-catenin and actin fibers at the cell-cell junctions. In α-catenin knockout cells, the expression of AJ-associated proteins and EGFR is not altered (Fig. S3B).

For patterned clusters of α-catenin knockout cells, addition of EGF to the culture media does not induce collective dynamics leading to rearrangement of the cluster as observed in A431 wildtype cells. Instead, individual cells extrude from the monolayer and adhere loosely on top of it. Cell traction forces for clusters of α-catenin knockout cells on micropatterned islands of different size were recorded over a period of 24 h following the addition of EGF to the media (Fig. 3A and Movie 3). Cell tractions slightly increase and appear evenly distributed underneath the entire cluster for all sizes, while no changes are observed in absence of EGF. Thus, the presence of intact AJs is necessary for the regulation of collective traction forces exerted to the substrate. In contrast, in absence of AJs between cells, the monolayer stress is slightly increased and randomly distributed in patches (Fig. 3A and Movie 3). Calculation of the average monolayer stress over time also shows a modest increase upon addition of EGF, however there is no correlation of internal stress levels with the cluster size. No changes were monitored for micropatterned α-catenin knockout cell clusters in absence of EGF.

Supplementary material related to this article can be found online at doi:10.1016/j.ejcb.2022.151274.

Rescue transfection with α-catenin restores the collective response to EGF in knockout cells and dome-like clusters are observed (Fig. 3B and Movie 3), suggesting that AJs are crucial for force transmission and increase, as observed in Fig. 2. A ring-like distribution of traction forces and internal stresses is observed and the average value is higher in comparison to α-catenin knockout cells (Fig. 3B and Movie 3). In these cell clusters, not only does the average internal stress increase to a level comparable to the A431 wildtype cells (Fig. 2B), but also the correlation between size and stress is maintained. Taken together these results indicate that AJs are crucial for the collective response to EGF-induced contractility by regulating the distribution of forces at cell-cell and cell-matrix adhesions.

3.4. A reinforcement in cell-matrix adhesions counteracts EGF-induced collective retraction of cell clusters

We next monitored the temporal changes in actin organization in cell clusters at different time points during the first 90 min following addition of EGF to the culture media (Fig. 4A). Actin fibers visualized by SiR-actin labelling are visible at the border of the cluster in a belt-like structure prior to addition of EGF (indicated as 0 min). The change in actin network organization, characterized by the presence of retracting fibers in cells at the cluster periphery, is observed already within the first 5 min after addition of the growth factor (Movie 4). After 60 min, the initial local retractions lead to a collective response, i.e. groups of cells at the periphery move towards the cluster center and actin fibers appear densely packed and disorganized (Fig. 4A zoom in boxes and Movie 4). For 300 μm and 200 μm clusters (Fig. 4A first and second row), localized contraction of cell groups are visible (white arrows) whereas for smaller clusters a global response is more evident, as shown by increased fluorescence intensity of actin at the periphery of the cluster, leading to an overall decrease in cluster size (Fig. 4A third row). Since cell-generated contractile forces are important for the maintenance of cell-cell contacts

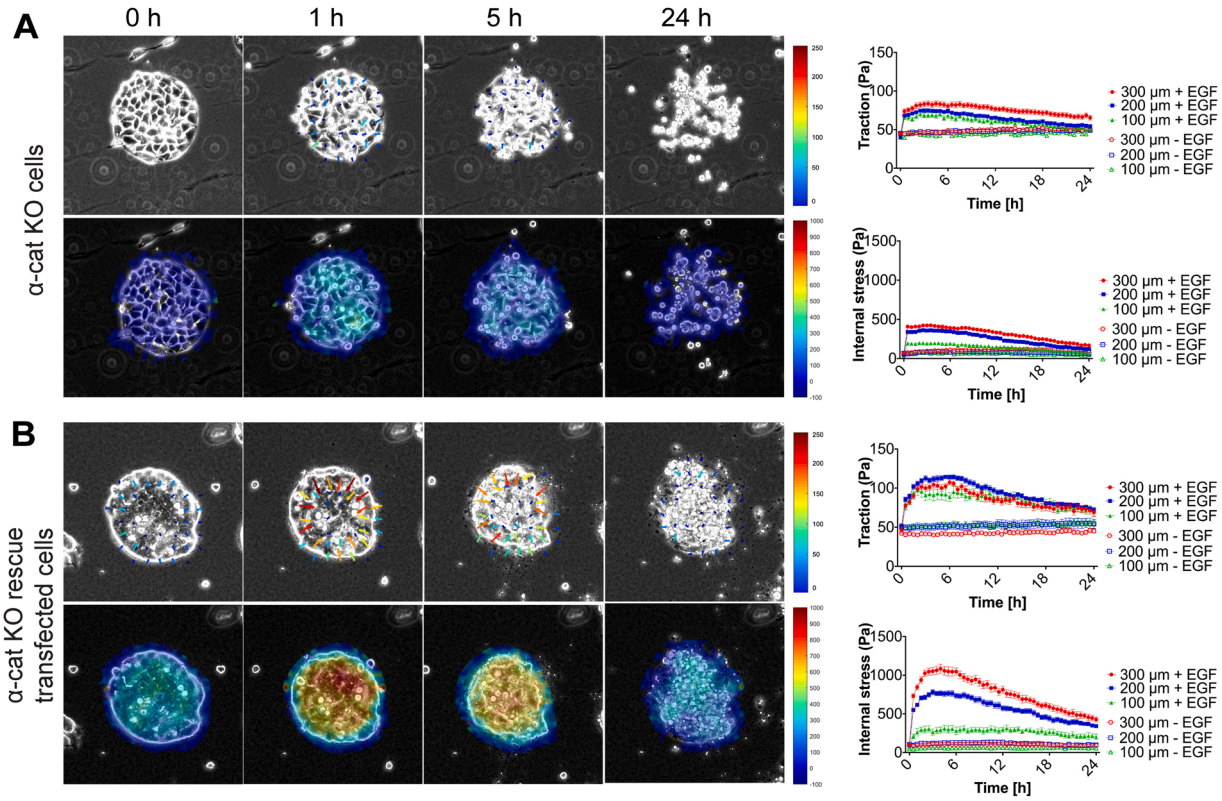

Fig. 3. Adherens junctions are crucial for distribution of actomyosin contractility within cell clusters. Traction force maps and internal stress overlay on cell clusters of 200 µm diameter. **A,** Traction force microscopy and internal stresses of α-catenin KO cells adhering to micropatterned 6 kPa PAA hydrogels. Plot indicates the tractions over time of three cluster sizes. N = 9, 17, 6 for 300, 200, 100 µm clusters in control condition (− EGF) and n = 16, 20, 17 for 300, 200, 100 µm clusters in presence of EGF stimulation (+ EGF). Data from 2 independent experiments. **B,** Traction forces and internal stresses of Cherry-α-catenin rescue transfected α-catenin KO cells tractions plotted over time. N = 7, 10, 9 for 300, 200, 100 µm clusters − EGF, while N = 8, 13, 6 for 300, 200, 100 µm clusters + EGF. Scale bar 100 µm.

and organization of cell collectives, we probed the involvement of myosin II-dependent contractility in 100 µm cell cluster reorganization in response to EGF (Fig. 4B). Before addition of EGF, cells were treated for 1 h with blebbistatin, a specific inhibitor of myosin II head binding to actin. Over a 30-min period after inhibition of actomyosin contractility, cell cluster area remains unchanged. Addition of EGF leads to increase in contractility and decrease in cell cluster area only in absence of blebbistatin, whereas for clusters pre-treated with the drug, the area does not decrease significantly during the 30-min observation period after addition of EGF to the culture media (Fig. 4B). The slight change in cluster area might be due to the direct perturbation of proteins which localize at focal adhesion in a myosin II dependent manner (Pasapera et al., 2010).

Supplementary material related to this article can be found online at doi:10.1016/j.ejcb.2022.151274.

Since EGF induces the phosphorylation of myosin II heavy chains and the maintenance of cell-cell and cell-matrix adhesion is tightly coupled to actomyosin contractility (Schneider et al., 2009), we stained cell clusters for AJs, FAs and the actin cytoskeleton (Fig. 4C). After 30-min addition of EGF to the media, in absence of blebbistatin cells present distinct E-cadherin localization at cell-cell contacts and robust FAs, as evidenced by zyxin clusters at the periphery and within the group of cells. In presence of blebbistatin, cell-cell contacts are preserved but present a disorganized localization of E-cadherins at the junctions; cell-matrix adhesions and actin stress fibers are reduced and partly disrupted (Fig. 4C). These results indicate that actomyosin contractility is essential for the changes in cell cluster organization and dynamics in response to EGF and suggest that such changes impact cell-cell and cell-matrix adhesion sites.

3.5. The reinforcement of cell-matrix adhesions is due to increased tension at the cluster periphery

In response to EGF-induced contractility, actin stress fiber organization leads to enlarged matrix adhesions, which are disrupted by blebbistatin treatment for all cell clusters sizes (Fig. S5). To determine whether EGF-induced changes in FAs at the periphery of cell clusters are related to epithelial collective tension, we investigated the distribution of actin and phosphorylated myosin light chain (pMLC) in epithelial cell clusters treated with EGF (Fig. 5). At the molecular level, the mechanical coupling between integrin β1-mediated adhesions and the contractile cell actomyosin cortex is mediated by MLC phosphorylation (Chugh et al., 2017; Truong Quang et al., 2021), which could be EGF-dependent (Petrov et al., 2017). In absence of EGF, actin fibers are organized tangential to the border at the periphery of all epithelial cluster sizes. pMLC is mainly present at the border with the passivated area surrounding the clusters and integrin β1 in the form of diffuse small aggregates(Fig. 5A, upper row). Following addition of EGF, actin stress fibers become very evident and they are coupled to elongated integrin β1 clusters (Fig. 5A inserts); pMLC is more pronounced at the border of all clusters and proximal to integrin β1 clusters (Fig. 5A second row). For all epithelial cell clusters, the rearrangement due to addition of EGF leads to a strong peripheral change and the FAs appear more radially distributed in comparison to the clusters which were not treated with EGF (Fig. 5A inserts). Analysis of integrin β1 cluster size and elongation indicates that FAs do not differ in size, but they are more elongated in cells at the periphery of the 300 µm cluster. Only after addition of EGF, a radial reorientation of integrin β1 clusters due to centripetal sliding of adhesions is observed, without evident rupture of integrin-mediated adhesions (Fig. 5B).

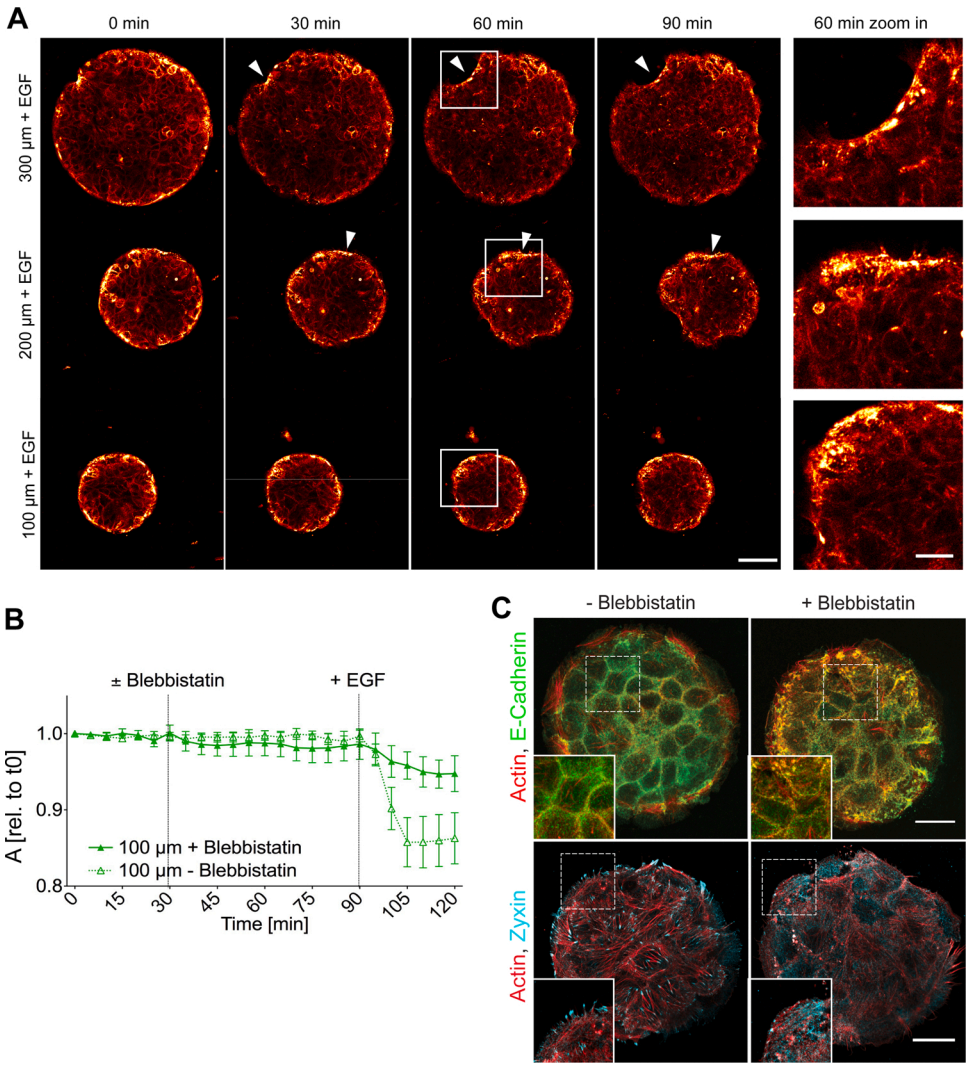

Fig. 4. Inhibition of actomyosin contractility prevents changes in cluster area and perturbs adherens junction and focal adhesion organization in EGF treated cells. A, Confocal images of representative clusters treated with EGF and labelled with SiR-actin for actin stress fibers; scale bar 50 µm; zoom in scale bar 15 µm. **B**, 100 µm cluster area quantification over time following addition of blebbistatin (30 min) and EGF (90 min) after initial observation. Samples treated with only DMSO (– blebbistatin) and EGF served as control. N = 28 and 23 for – and + blebbistatin respectively, from 3 different experiments. Plots display mean ± SD. **C**, 100 µm -sized clusters stained for adherens junctions (top) and focal adhesions (bottom) marker proteins 30 min after EGF treatment. The localization of E-cadherin (green), zyxin (cyan), actin stress fibers (red) in A431 cells is shown in maximum projections of z-stack confocal images. White boxes are 2x zoom in for selected regions of the cluster. Scale bar 20 µm.

We next monitored focal adhesion dynamics in single cells expressing fluorescently tagged-paxillin (Fig. 6A and Movie 5). Within the first 5 min after addition of EGF, cells in clusters show an increase in paxillin fluorescence signal, which is maintained over a period of 15 min and then drops to the initial levels at 30 and 60 min (Fig. 6B). Such increase in signal is accompanied by the translocation of paxillin-rich structures, as shown in the kymographs displaying fluorescence intensity values (Fig. 6C).

Supplementary material related to this article can be found online at doi:10.1016/j.ejcb.2022.151274.

In absence of intact AJs in A431 α-catenin knockout cells, addition of EGF still leads to the assembly of larger FAs associated with robust stress fibers at the periphery of cell clusters (Fig. S6). In summary, the radial contraction and dome-like reorganization are due to transmission of forces at cell-matrix junctions, where tension is key for contractility. As such, EGF-induced changes in collectives involve dramatic structural changes at the periphery of epithelial clusters.

4. Discussion

The objective of this study was to investigate EGF-induced changes in collective dynamics of epithelial cells. To obtain defined cluster sizes, we confined cells in 100–200–300 µm-wide circular micropatterns. The addition of EGF to the culture medium led to a rapid contraction of all clusters. The EGF-induced contractile forces of the epithelial clusters were measured by using traction force microscopy. The analysis of their radial distribution showed that tractions were highest at the border of the cluster and progressed inwards. Through stress inference, we observed an overall increase in epithelial tissue compressive stress upon EGF addition only in presence of intact cell-cell junctions. Here, a cooperativity between cells in the clusters contributes to building up contractile stresses that induce a redistribution of traction force to the periphery of the clusters, which scales with cluster size. Since FAs at the edge are subjected to increased forces, they undergo reinforcement which could be explained by a molecular clutch mechanism (Elosegui-Artola et al., 2018). The following detachment due to high tension, would lead to cluster retraction and two-dimensional to three-dimensional transitions as a result of internal contractility of the tissue.

How the regulation of EGF-induced contractility in epithelial cell collectives leads to arrangement of matrix adhesions, redistribution of forces and stresses might depend on two aspects. The first one is represented by the long-range interactions between epithelial cells organized in clusters of different sizes. In the present study, within the first two hours, the EGF-induced contractility of epithelial cell collectives is independent of the cluster size (Fig. 1). However, the subsequent dynamics of the cluster appear to be regulated by cluster size. It should be noted that our study does not address the direct contribution of cell number within the clusters to force generation, but it might be possible that more cells, and therefore increased cell-cell connections, could also

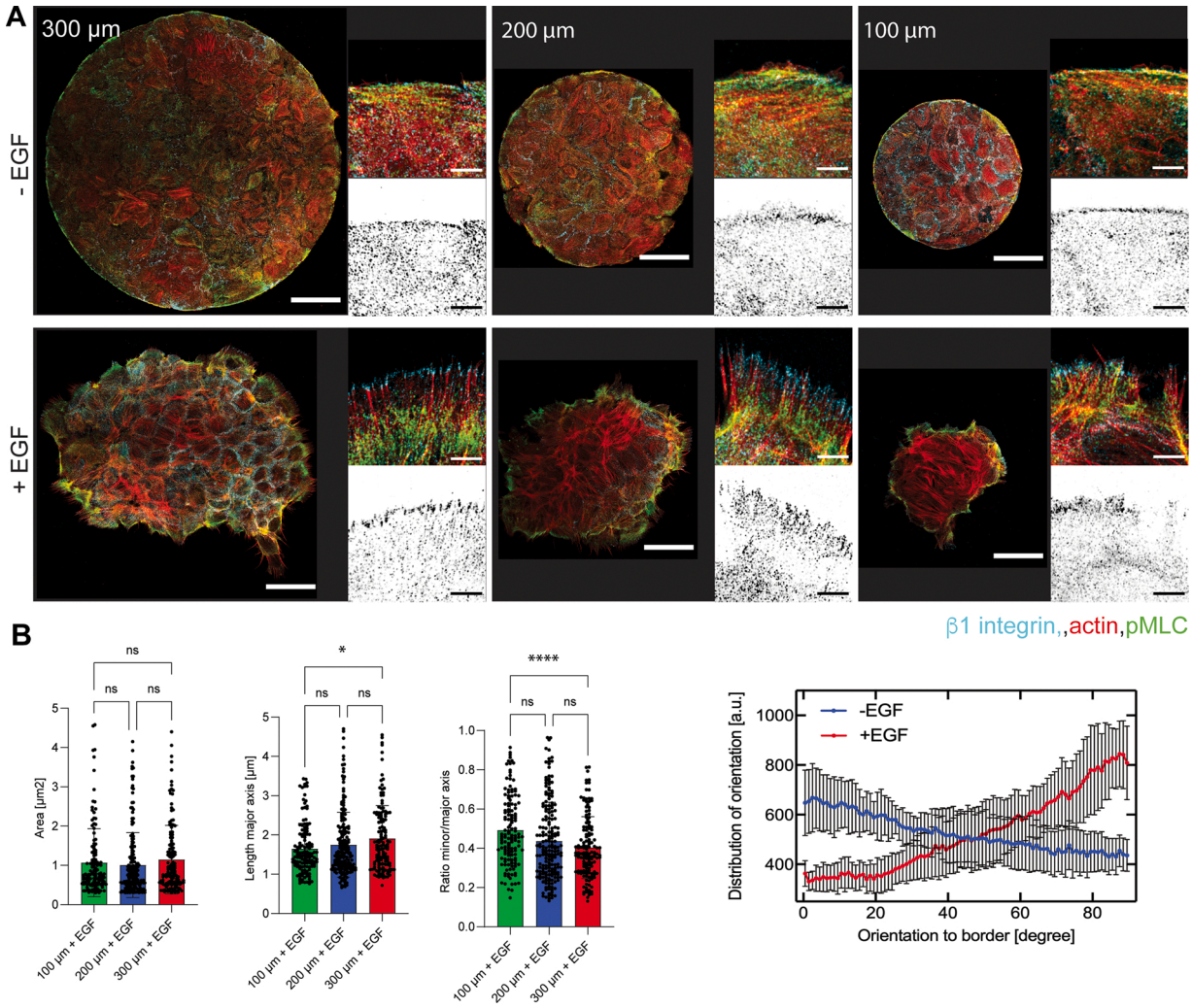

Fig. 5. EGF-induced contractility increases peripheral tension and focal adhesions. A, Representative confocal images of cell clusters adhering to micropatterns of different size treated or not with EGF. Cells were fixed 1 h after addition of 100 ng/ml EGF and immunostained for pMLC2 (green), F-actin (red) and integrin β1 (cyan). Inserts of inverted grayscale images of integrin β1. Scale bar 20 µm for cluster overview; 5 µm for inserts. **B,** Quantification of integrin β1 cluster area, length and aspect ratio in cells at the periphery of micropatterns of different sizes after addition of EGF. Analysis of integrin β1 cluster orientation angle relative to the cell cluster border for all patterns of different size treated or not with EGF.

cooperate to reach higher levels of internal stresses and tractions at the cluster edge. Nevertheless, our results are in line with previous observations on wetting transitions induced by increased collective contractility. The retraction of epithelial monolayers into three-dimensional aggregates has been studied in terms of a dewetting phenomenon (Beaune et al., 2018; Douezan et al., 2012, 2011; Nyga et al., 2021; Perez-Gonzalez et al., 2019; Wallmeyer et al., 2018). In this physical framework, the epithelium is interpreted in terms of a subset of coarse-grained variables. In the first models, the ability of a tissue to wet or dewet a surface is viewed in frame of competition between cell-cell and cell-substrate adhesion energies (Douezan et al., 2012, 2011). In later developments, additional variables were introduced to account for the active nature of the tissue (Nyga et al., 2021; Perez-Gonzalez et al., 2019). These variables including traction, contractility, viscosity and friction. The link between these coarse grained variables and the molecular elements of the cells remains unknown. Our study contributes to bridge this gap by showing that the process of dewetting induced by EGF involves dramatic reorientations in stress bearing subcellular components at the cluster periphery.

An additional aspect to consider is the distinct EGF activity at cell-cell and cell-matrix adhesions at the molecular level. At AJs, E-cadherin lateral mobility and activity is controlled by cortical actomyosin forces (Chiasson-MacKenzie et al., 2015). Treatment with EGF dissociates actin and vinculin from the E-cadherin-catenin complex in MDA-MB468 cells, which do not express α-catenin, resulting in increased tyrosine phosphorylation of the β-catenin/p120 complex at AJs (Hazan and Norton, 1998). Therefore, the presence of α-catenin appears to be crucial for the maintenance of AJs following EGF-induced contractility in epithelial cell collectives. Our results with the α-catenin knockout A431 rescue transfected indicate that α-catenin is required for the peripheral increase in traction forces in all cluster sizes and, as expected, for the resulting generation of intercellular stresses (Fig. 3). Similarly, previous studies on the influence of intercellular adhesions on cell traction forces evidenced that colonies of keratinocytes in absence of AJs present disorganized forces throughout the colony; and restoring strong cadherin-mediated adhesions results in peripheral traction forces (Mertz et al., 2013). The modest increase in tractions observed in the α-catenin knockout cells does not follow the radial pattern we observed when intact AJs are formed (Figs. 2 and 3B), and it can be attributed to EGF-induced contractility and increase in cell-matrix adhesions in isolated cells (Fig. S5). The force transduction pathways at E-cadherin-mediated junctions involve a strengthening of the α-catenin-actin linkage resulting in increased tractions. However, α-catenin is not the only regulator of contractility responses, since activation of EGFR is

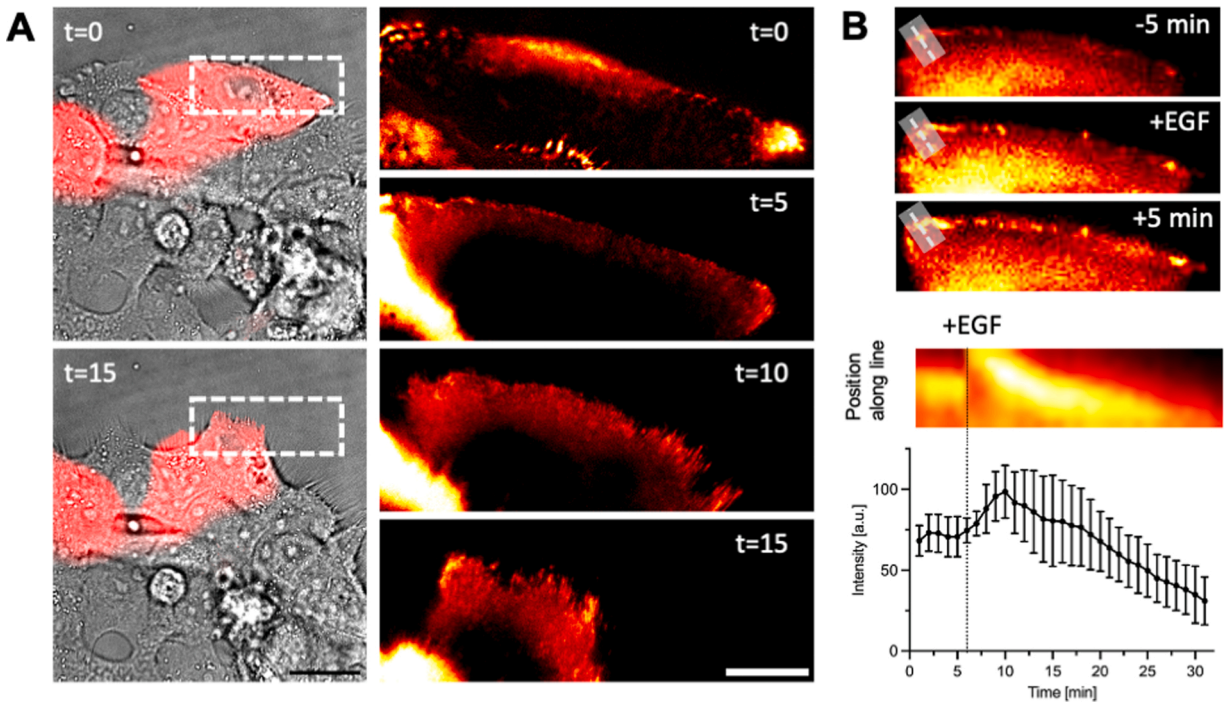

Fig. 6. EGF-induced actomyosin contractility leads to an initial transient reinforcement of focal adhesions. A, Representative image of a A431 cell at the periphery of a 200 μm cluster. Cells were transfected with paxillin-YFP and imaged 5 min before EGF stimulation and 1 h after. Left, overlay of polarized and fluorescence images at addition of EGF and 15 min after, scale bar 25 μm. The white box indicates the ROI, selected time points are displayed with a red hot color intensity. Scale bar 10 μm. **B,** Average kymograph and signal intensity analysis of paxillin clusters (line 8 pixel wide). Signal intensity measured along the ROI plotted for the different time points. Kymograph of the ROI was calculated for complete time lapse. Dashed line indicates the addition of EGF. N = 8 from 2 different cell clusters.

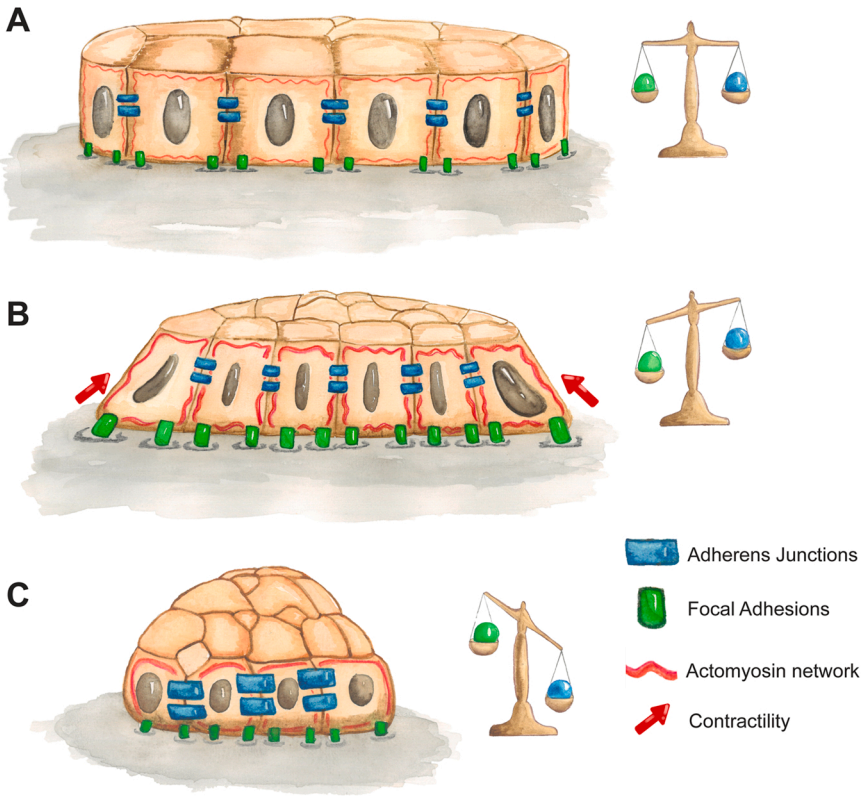

Fig. 7. Working model for the regulation of cell-matrix and cell-cell adhesion forces following EGF-induced actomyosin contractility. A, A cluster of cells grown in micropatterns is maintained as a monolayer through a balance of forces at focal adhesions and adherens junctions. **B,** Following EGF-induced actomyosin contractility, a rapid rearrangement and increase of traction forces at focal adhesions results in contraction of the cluster. **C,** Concomitantly, because of increasing forces at adherens junctions, cell-matrix adhesions can no longer sustain the contacts at the periphery. Further cluster contraction leads to a transition from two-dimensional into a three-dimensional cluster.

needed for myosin II dependent increase of cell stiffness (Barry et al., 2014; Muhamed et al., 2016).

Several growth factors regulate cell-ECM adhesion by mechanisms that act on integrin expression, activation and focal adhesion turnover. Nevertheless, this alone cannot explain the reduction in cell-ECM binding in epithelial cancer cells and their invasive behavior. EGF stimulates an increase in actin assembly at the leading edge and lamellipodia extensions and regulates mDia1 activation in MDA-MB231 cells (Isogai et al., 2015) and inhibition of EGFR increase the basal level of Rac activation in keratinocytes (Betson et al., 2002). EGF increases FA size and integrin tension in adherent cells, suggesting that its receptor might regulate integrin activation (Rao et al., 2020). We observed elongated integrin β1 clusters in cells at the micropattern periphery and an increase in pMLC after addition of EGF. Integrin engagement at the cell cluster peripheries is independent of micropattern size (Fig. 5A); however only for all cell clusters treated with EGF, integrin β1 clusters rapidly elongate towards the center of the cell cluster and reorient radially, suggesting their mechanical activation by cytoskeletal contractility. Integrin-mediated adhesions generate high forces to the substrate, and a size threshold of approximately 0.1 μm^2 has been previously identified to be necessary for stability and efficient force transmission (Coyer et al., 2012). However, for cell clusters not treated with EGF, we could not appreciate any evident reorganization of the small FAs, and we reasoned that this lack in reinforcement and force transmission might be due to the stabilization of AJs. Overall, our results can be interpreted through the balance between actomyosin contractility and adhesion reinforcement, in the framework of the molecular clutch theory (Elosegui-Artola et al., 2018) (Fig. 7). Once EGF triggers myosin phosphorylation and thereby contractility, increased force transmission to the substrate through focal adhesions leads to adhesion reinforcement and their growth (Elosegui-Artola et al., 2016). This will tend to slow the contraction of the cluster. However, forces continue to increase, reaching the point at which adhesions can no longer sustain them (Andreu et al., 2021), leading to adhesion disassembly. This further promotes cluster contraction, progressively converting the two-dimensional epithelial monolayer into a three-dimensional aggregate. As this occurs, the component of myosin contractility that acts along the 2D substrate plane becomes progressively smaller, eventually halting contraction and stabilizing the cluster. After this point, re-spreading of cells along the substrate slowly increases cluster size. In clusters with intact AJs, contractility is transmitted through the entire cluster. For increasing cluster size, total contractility (which depends on the total number of cells, and therefore scales with pattern surface) dominates over adhesions, which occur mainly at the periphery of the cluster and therefore scale with pattern perimeter. This explains the increased reduction in area for larger patterns, since surface effects will dominate over perimeter effects as size increases. Consistently with this, cluster contraction and size dependencies are lost upon α-catenin depletion.

5. Conclusions

In this work, we show that in response to EGF actomyosin contractility is essential for epithelial cell cluster organization and dynamics and such changes impact cell-cell and cell-matrix adhesion sites. The size of the epithelial cell cluster and the presence of cell-cell junctions lead the coordination of forces at the periphery upon EGF-induced retraction, resulting in a global rearrangement of the collective.

CRediT authorship contribution statement

C.Z. and E.A.C.A. Conceptualization; C.Z., C.P.G., C.S., A.S., N.V., R. J., D.O. and E.A.C.A. data acquisition and analysis; C.Z., C.P.G., A.S., N. V., R.J. and J.C. Methodology; C.Z., C.P.G., A.S., E.A.C.A Visualization; E.A.C.A. Project administration; E.A.C.A and X.T. Resources; E.A.C.A., P. R.C., X.T. Supervision. E.A.C.A and X.T. Writing – original draft; all authors: Writing – review & editing.

Funding

This work was supported by the Max Planck Society (E.A.C.A.), Baden Württemberg Stiftung (3D-MOSAIC to E.A.C.A.), Generalitat de Catalunya (Agaur, the CERCA Programme, and "ICREA Academia" to P. R-C.), Spanish Ministry for Science and Innovation MICCINN/FEDER (PGC2018-099645-B-I00 to X.T., 110298GB-I00 to P. R.-C), European Research Council (Adv-883739 to X.T), European Commission (H2020-FETPROACT-01-2016-731957 to P.R-C.) and La Caixa Foundation (LCF/PR/HR20/52400004).

Competing interests

The authors declare no competing interests.

Data Availability

Data will be made available on request.

Acknowledgements

We thank the members of the E.A.C-A. and X.T. laboratories, R-M. Mege and A. Deutsch for fruitful discussions. We thank Dr. Takuya Kato (the Francis Crick Institute) for providing the a-catenin Crispr/Cas9 cell lines and Dr. Carlo Beretta (CellNetworks Math-Clinic) for support in setting the traction force data analysis tool. We acknowledge the Cellular Biotechnology facility of MPImR for FACS support. C.Z. and D. O. were former student members of the Heidelberg Biosciences International Graduate School (HBIGS), Heidelberg University.

Data Availability

The authors declare that the data supporting the findings of this study are available within the paper and its Supplementary information files.

Appendix A. Supporting information

Supplementary data associated with this article can be found in the online version at doi:10.1016/j.ejcb.2022.151274.

References

Andreu, I., Falcones, B., Hurst, S., Chahare, N., Quiroga, X., Le Roux, A.L., Kechagia, Z., Beedle, A.E.M., Elosegui-Artola, A., Trepat, X., Farre, R., Betz, T., Almendros, I., Roca-Cusachs, P., 2021. The force loading rate drives cell mechanosensing through both reinforcement and cytoskeletal softening. Nat. Commun. 12, 4229.

Arganda-Carreras, I., Kaynig, V., Rueden, C., Eliceiri, K.W., Schindelin, J., Cardona, A., Sebastian Seung, H., 2017. Trainable Weka Segmentation: a machine learning tool for microscopy pixel classification. Bioinformatics 33, 2424–2426.

Azioune, A., Carpi, N., Tseng, Q., Théry, M., Piel, M., 2010. Protein micropatterns. Microtubules: In Vivo, pp. 133–46.

Barry, A.K., Tabdili, H., Muhamed, I., Wu, J., Shashikanth, N., Gomez, G.A., Yap, A.S., Gottardi, C.J., de Rooij, J., Wang, N., Leckband, D.E., 2014. alpha-catenin cytomechanics–role in cadherin-dependent adhesion and mechanotransduction. J. Cell Sci. 127, 1779–1791.

Beaune, G., Blanch-Mercader, C., Douezan, S., Dumond, J., Gonzalez-Rodriguez, D., Cuvelier, D., Ondarcuhu, T., Sens, P., Dufour, S., Murrell, M.P., Brochard-Wyart, F., 2018. Spontaneous migration of cellular aggregates from giant keratocytes to running spheroids. Proc. Natl. Acad. Sci. USA 115, 12926–12931.

Betson, M., Lozano, E., Zhang, J., Braga, V.M., 2002. Rac activation upon cell-cell contact formation is dependent on signaling from the epidermal growth factor receptor. J. Biol. Chem. 277, 36962–36969.

Casares, L., Vincent, R., Zalvidea, D., Campillo, N., Navajas, D., Arroyo, M., Trepat, X., 2015. Hydraulic fracture during epithelial stretching. Nat. Mater. 14, 343–351.

Chiasson-MacKenzie, C., Morris, Z.S., Baca, Q., Morris, B., Coker, J.K., Mirchev, R., Jensen, A.E., Carey, T., Stott, S.L., Golan, D.E., McClatchey, A.I., 2015. NF2/Merlin mediates contact-dependent inhibition of EGFR mobility and internalization via cortical actomyosin. J. Cell Biol. 211, 391–405.

Chinkers, M., McKanna, J.A., Cohen, S., 1979. Rapid induction of morphological changes in human carcinoma cells A-431 by epidermal growth factor. J. Cell Biol. 83, 6.

Choi, C.K., Vicente-Manzanares, M., Zareno, J., Whitmore, L.A., Mogilner, A., Horwitz, A.R., 2008. Actin and alpha-actinin orchestrate the assembly and

maturation of nascent adhesions in a myosin II motor-independent manner. Nat. Cell Biol. 10, 1039–1050.
Chugh, P., Clark, A.G., Smith, M.B., Cassani, D.A.D., Dierkes, K., Ragab, A., Roux, P.P., Charras, G., Salbreux, G., Paluch, E.K., 2017. Actin cortex architecture regulates cell surface tension. Nat. Cell Biol. 19, 689–697.
Coyer, S.R., Singh, A., Dumbauld, D.W., Calderwood, D.A., Craig, S.W., Delamarche, E., Garcia, A.J., 2012. Nanopatterning reveals an ECM area threshold for focal adhesion assembly and force transmission that is regulated by integrin activation and cytoskeleton tension. J. Cell Sci. 125, 5110–5123.
De Vos, W.H.M.S., Timmermans, J.-P., 2016. Focus on Bio-Image Informatics. Springer.
Douezan, S., Guevorkian, K., Naouar, R., Dufour, S., Cuvelier, D., Brochard-Wyart, F., 2011. Spreading dynamics and wetting transition of cellular aggregates. Proc. Natl. Acad. Sci. USA 108, 7315–7320.
Douezan, S., Dumond, J., Brochard-Wyart, F., 2012. Wetting transitions of cellular aggregates induced by substrate rigidity. Soft Matter 8.
Elosegui-Artola, A., Oria, R., Chen, Y., Kosmalska, A., Perez-Gonzalez, C., Castro, N., Zhu, C., Trepat, X., Roca-Cusachs, P., 2016. Mechanical regulation of a molecular clutch defines force transmission and transduction in response to matrix rigidity. Nat. Cell Biol. 18, 540–548.
Elosegui-Artola, A., Trepat, X., Roca-Cusachs, P., 2018. Control of mechanotransduction by molecular clutch dynamics. Trends Cell Biol. 28, 356–367.
Felkl, M., Tomas, K., Smid, M., Mattes, J., Windoffer, R., Leube, R.E., 2012. Monitoring the cytoskeletal EGF response in live gastric carcinoma cells. PLoS One 7, e45280.
Han, M.K., Hoijman, E., Noel, E., Garric, L., Bakkers, J., de Rooij, J., 2016. alphaE-catenin-dependent mechanotransduction is essential for proper convergent extension in zebrafish. Biol. Open 5, 1461–1472.
Hazan, R.B., Norton, L., 1998. The epidermal growth factor receptor modulates the interaction of E-cadherin with the actin cytoskeleton. J. Biol. Chem. 273, 9078–9084.
Isogai, T., van der Kammen, R., Leyton-Puig, D., Kedziora, K.M., Jalink, K., Innocenti, M., 2015. Initiation of lamellipodia and ruffles involves cooperation between mDia1 and the Arp2/3 complex. J. Cell Sci. 128, 3796–3810.
Labernadie, A., Kato, T., Brugues, A., Serra-Picamal, X., Derzsi, S., Arwert, E., Weston, A., Gonzalez-Tarrago, V., Elosegui-Artola, A., Albertazzi, L., Alcaraz, J., Roca-Cusachs, P., Sahai, E., Trepat, X., 2017. A mechanically active heterotypic E-cadherin/N-cadherin adhesion enables fibroblasts to drive cancer cell invasion. Nat. Cell Biol. 19, 224–237.
Latorre, E., Kale, S., Casares, L., Gomez-Gonzalez, M., Uroz, M., Valon, L., Nair, R.V., Garreta, E., Montserrat, N., Del Campo, A., Ladoux, B., Arroyo, M., Trepat, X., 2018. Active superelasticity in three-dimensional epithelia of controlled shape. Nature 563, 203–208.
Makowiecka, A., Simiczyjew, A., Nowak, D., Mazur, A.J., 2016. Varying effects of EGF, HGF and TGFbeta on formation of invadopodia and invasiveness of melanoma cell lines of different origin. Eur. J. Histochem. 60, 2728.
Maruthamuthu, V., Sabass, B., Schwarz, U.S., Gardel, M.L., 2011. Cell-ECM traction force modulates endogenous tension at cell-cell contacts. Proc. Natl. Acad. Sci. USA 108, 4708–4713.
Mertz, A.F., Che, Y., Banerjee, S., Goldstein, J.M., Rosowski, K.A., Revilla, S.F., Niessen, C.M., Marchetti, M.C., Dufresne, E.R., Horsley, V., 2013. Cadherin-based intercellular adhesions organize epithelial cell-matrix traction forces. Proc. Natl. Acad. Sci. USA 110, 842–847.
Muhamed, I., Wu, J., Sehgal, P., Kong, X., Tajik, A., Wang, N., Leckband, D.E., 2016. E-cadherin-mediated force transduction signals regulate global cell mechanics. J. Cell Sci. 129, 1843–1854.
Mui, K.L., Chen, C.S., Assoian, R.K., 2016. The mechanical regulation of integrin-cadherin crosstalk organizes cells, signaling and forces. J. Cell Sci. 129, 1093–1100.
Notbohm, J., Kim, J.H., Asthagiri, A.R., Ravichandran, G., 2012. Three-dimensional analysis of the effect of epidermal growth factor on cell-cell adhesion in epithelial cell clusters. Biophys. J. 102, 1323–1330.
Nyga, A., Munoz, J.J., Dercksen, S., Fornabaio, G., Uroz, M., Trepat, X., Baum, B., Matthews, H.K., Conte, V., 2021. Oncogenic RAS instructs morphological transformation of human epithelia via differential tissue mechanics. Sci. Adv. 7, eabg6467.
Oakes, P.W., Beckham, Y., Stricker, J., Gardel, M.L., 2012. Tension is required but not sufficient for focal adhesion maturation without a stress fiber template. J. Cell Biol. 196, 363–374.
Pannekoek, W.J., de Rooij, J., Gloerich, M., 2019. Force transduction by cadherin adhesions in morphogenesis. F1000Res 8.
Pasapera, A.M., Schneider, I.C., Rericha, E., Schlaepfer, D.D., Waterman, C.M., 2010. Myosin II activity regulates vinculin recruitment to focal adhesions through FAK-mediated paxillin phosphorylation. J. Cell Biol. 188, 877–890.
Perez-Gonzalez, C., Alert, R., Blanch-Mercader, C., Gomez-Gonzalez, M., Kolodziej, T., Bazellieres, E., Casademunt, J., Trepat, X., 2019. Active wetting of epithelial tissues. Nat. Phys. 15, 79–88.
Petrov, D., Dahan, I., Cohen-Kfir, E., Ravid, S., 2017. aPKCzeta affects directed cell migration through the regulation of myosin light chain phosphorylation. Cell Adhes. Migr. 11, 347–359.
Rao, T.C., Ma, V.P., Blanchard, A., Urner, T.M., Grandhi, S., Salaita, K., Mattheyses, A.L., 2020. EGFR activation attenuates the mechanical threshold for integrin tension and focal adhesion formation. J. Cell Sci. 133.
Rubsam, M., Mertz, A.F., Kubo, A., Marg, S., Jungst, C., Goranci-Buzhala, G., Schauss, A. C., Horsley, V., Dufresne, E.R., Moser, M., Ziegler, W., Amagai, M., Wickstrom, S.A., Niessen, C.M., 2017. E-cadherin integrates mechanotransduction and EGFR signaling to control junctional tissue polarization and tight junction positioning. Nat. Commun. 8, 1250.
Schneider, I.C., Hays, C.K., Waterman, C.M., 2009. Epidermal growth factor-induced contraction regulates paxillin phosphorylation to temporally separate traction generation from de-adhesion. Mol. Biol. Cell 20, 3155–3167.
Seddiki, R., Narayana, G., Strale, P.O., Balcioglu, H.E., Peyret, G., Yao, M., Le, A.P., Teck Lim, C., Yan, J., Ladoux, B., Mege, R.M., 2018. Force-dependent binding of vinculin to alpha-catenin regulates cell-cell contact stability and collective cell behavior. Mol. Biol. Cell 29, 380–388.
Stricker, J., Aratyn-Schaus, Y., Oakes, P.W., Gardel, M.L., 2011. Spatiotemporal constraints on the force-dependent growth of focal adhesions. Biophys. J. 100, 2883–2893.
Tambe, D.T., Hardin, C.C., Angelini, T.E., Rajendran, K., Park, C.Y., Serra-Picamal, X., Zhou, E.H., Zaman, M.H., Butler, J.P., Weitz, D.A., Fredberg, J.J., Trepat, X., 2011. Collective cell guidance by cooperative intercellular forces. Nat. Mater. 10, 469–475.
Tambe, D.T., Croutelle, U., Trepat, X., Park, C.Y., Kim, J.H., Millet, E., Butler, J.P., Fredberg, J.J., 2013. Monolayer stress microscopy: limitations, artifacts, and accuracy of recovered intercellular stresses. PLoS One 8, e55172.
Trepat, X., Wasserman, M.R., Angelini, T.E., Millet, E., Weitz, D.A., Butler, J.P., Fredberg, J.J., 2009. Physical forces during collective cell migration. Nat. Phys. 5, 426–430.
Truong Quang, B.A., Peters, R., Cassani, D.A.D., Chugh, P., Clark, A.G., Agnew, M., Charras, G., Paluch, E.K., 2021. Extent of myosin penetration within the actin cortex regulates cell surface mechanics. Nat. Commun. 12, 6511.
Wallmeyer, B., Trinschek, S., Yigit, S., Thiele, U., Betz, T., 2018. Collective cell migration in embryogenesis follows the laws of wetting. Biophys. J. 114, 213–222.
Yang, R., Chen, J.Y., Xi, N., Lai, K.W., Qu, C., Fung, C.K., Penn, L.S., Xi, J., 2012. Characterization of mechanical behavior of an epithelial monolayer in response to epidermal growth factor stimulation. Exp. Cell Res. 318, 521–526.